



Deposited via The University of Sheffield.

White Rose Research Online URL for this paper:

<https://eprints.whiterose.ac.uk/id/eprint/226472/>

Version: Accepted Version

Article:

Yang, X., Zhang, Y., Tang, H. et al. (2025) Spring rapid temperature variability in Southern China: characteristics, decadal trend and associated climate impacts on crop yield.

International Journal of Climatology, 45 (9). e8880. ISSN: 0899-8418

<https://doi.org/10.1002/joc.8880>

© 2025 The Authors. Except as otherwise noted, this author-accepted version of a journal article published in International Journal of Climatology is made available via the University of Sheffield Research Publications and Copyright Policy under the terms of the Creative Commons Attribution 4.0 International License (CC-BY 4.0), which permits unrestricted use, distribution and reproduction in any medium, provided the original work is properly cited. To view a copy of this licence, visit <http://creativecommons.org/licenses/by/4.0/>

Reuse

This article is distributed under the terms of the Creative Commons Attribution (CC BY) licence. This licence allows you to distribute, remix, tweak, and build upon the work, even commercially, as long as you credit the authors for the original work. More information and the full terms of the licence here:

<https://creativecommons.org/licenses/>

Takedown

If you consider content in White Rose Research Online to be in breach of UK law, please notify us by emailing eprints@whiterose.ac.uk including the URL of the record and the reason for the withdrawal request.

1 **Spring Rapid Temperature Variability in Southern China:**
2 **Characteristics, Decadal Trend and Associated Climate**
3 **Impacts on Crop Yield**

4 **Xianke Yang¹, Yixuan Zhang, Haosu Tang³, Ping Huang², Xiaoxia Ling¹, Shaobing**
5 **Peng¹, Dongliang Xiong¹**

6

Abstract

Climate-related risks are shaped not only by changes in mean temperatures, but also by temperature variability, which increases the probability of weather extremes and exerts profound impacts on society and ecosystems. Previous studies have documented contrasting seasonal trend differences in summer and winter temperature variability. However, spring temperature variability—a transitional period critical for agricultural production—has received limited attention. Using three indices, namely the standard deviation of daily temperature (STD), day-to-day temperature variability (DTD), and rapid cooling events (RCE), we analyze the decadal trends and drivers of spring temperature variability and quantify its effects on rice yield anomalies. Our findings reveal consistent trends in the spatial distribution of temperature variability, with increasing frequency and intensity in the Yangtze River Basin and Yunnan Province, and a decreasing trend across much of South China, closely following regional climatological patterns. Overall, the frequency and intensity of RCE trend exhibit a ‘stronger getting weaker, weaker getting stronger’ pattern, likely linked to increased STD trends driven by spatial non-uniformity of warming. Through a multiple regression statistical model, we find that climate factors, including mean climate and climate variability, explained 19%–49% of the variance in yield anomalies, with up to 11% of the explained variance attributable to spring temperature variability. This study underscores the critical role of spring temperature variability in climate resilience, informing strategies to enhance the adaptability of agricultural systems to extreme climate events.

30 **1. Introduction**

31 Climate change risks arise not only from growing mean temperatures but also from
32 shifts in temperature variability (Olonscheck et al. 2021; Van Der Wiel and Bintanja
33 2021). It is well known that short-term temperature variability affects both human
34 health and natural ecosystems. For instance, enhanced daily temperature variability has
35 been associated with increased mortality rate (Healy et al. 2023; Pane and Davis 2024).
36 Moreover, temperature variability modulates the frequency and intensity of extreme
37 climate events, such as heat waves or droughts, exerting severe impacts on ecosystems
38 and agriculture (Ray et al. 2015; Vogel et al. 2019; Kotz et al. 2021; Lesk and
39 Anderson 2021; Heinicke et al. 2022). While most existing studies have analyzed trends
40 and impacts related to mean temperature changes (Alexander 2016; Li and Thompson
41 2021; Rezaei et al. 2023; Samset et al. 2023), the changes in short-term temperature
42 variability, alongside the mechanisms driving these changes, have received
43 comparatively limited attention. Understanding this variability is crucial for elucidating
44 the long-term relationships between climate variability and extreme climate events,
45 facilitating better-informed decision-making in climate change mitigation.

46 Previous studies on short-term temperature variability reveal significant seasonal
47 differences. Reductions in temperature variability have been observed over high-
48 northern latitudes in autumn (Screen 2014; Blackport et al. 2021) and mid-latitudes in
49 winter (Schneider et al. 2015; Rhines et al. 2017), leading to fewer extreme cooling
50 events in these seasons (Cui and He 2023; He et al. 2023). On the contrary, summer
51 temperature variability has increased over most land areas, especially in Eurasia,
52 southern China and tropical zones (Chan et al. 2020; Xu et al. 2020; Krauskopf and
53 Huth 2024), exacerbating extreme heatwave events in recent decades (Schär et al. 2004;
54 Perkins-Kirkpatrick and Gibson 2017; Wei et al. 2023). Climate model simulations also
55 support these findings, revealing a decreasing trend in winter temperature variability
56 and an increasing trend in summer temperature variability at mid-latitudes (Holmes et
57 al. 2016; Bathiany et al. 2018; Tamarin-Brodsky et al. 2020). Mechanisms underlying
58 these changes in temperature variability have been attributed to multiple physical
59 processes, including meridional temperature gradients linked to Arctic amplification
60 (Screen 2014; Bathiany et al. 2018; Dai and Deng 2021), soil moisture–temperature

61 feedbacks (Fischer et al. 2012), and local warming pattern (Chan et al. 2020; Tamarin-
62 Brodsky et al. 2020).

63 However, insufficient attention has been paid to spring temperature variability. As
64 a transitional season from cold to warm, spring plays a crucial role in agricultural
65 production (Allstadt et al. 2015; Zhu et al. 2018). On one hand, it marks the harvest
66 season for winter cereal crops in crop rotation systems (e.g., rapeseed-rice, winter
67 wheat-rice); on the other hand, it serves as the sowing season for summer cereals (e.g.,
68 early rice, spring maize, spring wheat). Despite advancements in spring plant
69 phenology under global warming, the risk of a ‘false spring’ is increasing (Allstadt et
70 al. 2015; Chamberlain et al. 2019; Garner and Duran 2024). This phenomenon occurs
71 when temperatures fluctuate rapidly from warm to cold anomalies, characterized by
72 rapid cooling events and late spring cold spells (Xiao et al. 2018; Lin et al. 2023). Such
73 rapid temperature variability can severely affect the growth, health, competitive ability,
74 and geographical distribution limits of crops, ultimately leading to reduced crop yields.
75 Previous studies revealed that climate factors account for more than one-third of the
76 variations in global crop yield variability (Ray et al. 2015; Ray et al. 2019; Baffour-Ata
77 et al. 2021), with 18%–43% of the explained variance attributable to climate extremes
78 (Vogel et al. 2019). While it has been established that climate variability significantly
79 affects crops during the growing season, the impact of rapid temperature variability in
80 the special season remains underexplored.

81 As a major agricultural country, China is the world's largest producer of rice and
82 wheat and the second-largest producer of maize, contributing 27%, 17%, and 24% of
83 global production, respectively (FAO, 2023). The southern China is the core area for
84 the rotational cropping system and the primary rice-growing region, where rice
85 accounts for more than 70% of the national cultivation area (Figure 1a). Given the
86 importance of southern China in food production, understanding the characteristics and
87 impacts of climate variability in this region is crucial. However, relatively little
88 attention has been paid to the transition season in the main grain-producing regions in
89 the southern China. In particular, the decadal trends and impacts of spring temperature
90 variability remain unclear, limiting comprehensive analyses of climate-related disaster
91 impacts in this region.

92 In the present work, we aim to address the following questions through statistical
93 analyses of long-term observations: 1) What are the observed changes in spring
94 temperature variability, and 2) what mechanisms drive these changes? 3) To what
95 extent does spring temperature variability affect crop production? Here, we present a
96 comprehensive understanding of observed changes in spring temperature variability
97 over the past half-century, identifying causal factors and quantifying the impact on crop
98 yields. Our findings unveil a distinct pattern in the frequency and intensity of spring
99 rapid cooling events, characterized by ‘stronger getting weaker, weaker getting
100 stronger’. This pattern is potentially related to the increased standard deviation trend
101 caused by spatially uneven warming. Spring temperature variability can affect crop
102 production through cold spells, precipitation, and gusty winds, explaining up to 8% of
103 the variation in rice yields.

104 The rest of the paper is organized as follows. The datasets and methods are
105 described in Section 2. Section 3 details the climatological distribution of rapid
106 temperature variability. Section 4 explores decadal trends and underlying mechanisms
107 of rapid temperature variability changes. Section 5 outlines effects of this variability on
108 climate variations and crop yields. Finally, conclusion and discussion are given in
109 Section 6.

110 **2. Datasets and methods**

111 2.1 Datasets

112 The climate variables used in this study were sourced from the National Meteorological
113 Information Center of China Meteorological Administration, including daily
114 minimum and mean temperature, precipitation, and wind data from 1961 to 2023 at
115 over 2400 meteorological stations. The dataset has undergone rigorous quality control
116 and homogenization and is widely used in the study of climate extremes in China (Cao
117 et al. 2016; Han et al. 2024). To ensure consistency, stations with more than 30 days of
118 missing data or relocations exceeding 100 meters were excluded, resulting in a selection
119 of 587 stations in southern China (Figure 1b, colored dots). The selected stations en-
120 compass the majority of rice-growing regions and rotational cropping system areas in

121 China, spanning 13 provinces: Sichuan, Chongqing, Hubei, Anhui, Jiangsu, Guizhou,
122 Henan, Jiangxi, Zhejiang, Yunnan, Guangxi, Guangdong and Fujian.

123 In addition, the yearly provincial rice planting areas and yields were obtained from
124 the National Bureau of Statistics of China for the period of 1970–2022. Due to the
125 inconsistency in the time span of the meteorological and yield data, the period from
126 1970 to 2022 was used to analyze the trend and effects of rapid temperature variability.

127 2.2 Definition of rapid temperature variability

128 Three methods are used here to quantify rapid temperature variability. Firstly,
129 standard deviation of daily temperature (STD), calculated as the standard deviation of
130 daily mean temperature, is a widely used measure of rapid temperature variability
131 (Blackport et al. 2021; Cui and He 2023; Krauskopf and Huth 2024). In addition, day-
132 to-day temperature variability (DTD) is also used to measure rapid temperature vari-
133 ability, which is defined as the absolute difference in daily temperatures between two
134 adjacent days (Gough 2008; Xu et al. 2020; Ge et al. 2022), expressed as:

$$135 \quad DTD = \frac{1}{n} \sum_{i=1}^n | T_{i+1} - T_i |$$

136 Where T_i denotes 2-meter temperature on day i , and n denotes the total days.

137 Although both STD and DTD can describe temperature variability, DTD is more
138 representative than STD at describing the daily temperature change, particularly for dis-
139 tinguishing between orderly and oscillatory climates. For example, consider two daily
140 temperature series: an orderly series (e.g., 25, 25, 25, 25, 15, 15, 15, 15 °C) and an
141 oscillatory series (e.g., 25, 15, 25, 15, 25, 15, 25, 15 °C). Despite both having the same
142 STD value (5.27 °C), they exhibit a significant difference in DTD (1.25 °C versus

143 8.75 °C). This makes DTD more effective at capturing rapid temperature variability in
144 both orderly and oscillatory climate behaviors.

145 In addition to STD and DTD, rapid cooling event (RCE) was used to quantitatively
146 characterize the frequency and intensity of daily temperature variability. Based on the
147 absolute and relative thresholds, two types of definitions were used to identify RCE.
148 For the relative threshold method, the day-to-day temperature difference (ΔT) was first
149 calculated, and the relative threshold was defined as the 95th percentile from 1970 to
150 2022. Then, the RCE was identified when daily ΔT falls below the relative threshold.
151 For the absolute threshold method, the RCE was selected as ΔT below -6 °C, which
152 matches the threshold used in previous studies (Park et al. 2011; Cui and He 2023).
153 More importantly, the mean relative threshold across the 836 stations in southern China
154 is close to -6 °C. The frequency, mean intensity, and extreme intensity of RCE are
155 calculated as:

$$156 \quad \text{Frequency}_j = \sum_{i=1}^M \delta_{i,j}$$

$$157 \quad \text{Mean intensity}_j = \frac{\sum_{i=1}^M \delta_{i,j} * \Delta T_{i,j}}{\sum_{i=1}^M \delta_{i,j}}$$

$$158 \quad \text{Extreme intensity}_j = \text{Min}(\delta_{i,j} * \Delta T_{i,j})$$

159 Where δ is a symbolic function to judge RCE, in which $\delta_{i,j} = 1$ for days with an
160 RCE and $\delta_{i,j} = 0$ for days without an RCE. i denotes the day in special seasons, and j
161 denotes the year. $\sum()$ and $\text{Min}()$ indicate the sum and minimum value of the special
162 seasons, respectively. Here, both the mean and extreme intensity are multiplied by -1 to
163 express them as positive values for ease of interpretation.

164 2.3 Decadal trend and significant test

165 From the monthly and seasonal evolution of STD and DTD (Figure 2), it is clear
166 that the temperature variability in southern China is strongest in spring, with March
167 exhibiting significantly higher variability than other months. Meanwhile, given the im-
168 portance of spring in agricultural production, the present study focused on the charac-
169 teristics of spring temperature variability. The annual cycle of daily temperatures was
170 removed before calculating STD, DTD and RCE.

171 To ensure reliable estimation of temperature variability using abundant samples, an
172 11-year sliding window was applied for calculating decadal trends. STD, DTD and
173 RCE characteristics were calculated for each 11-year period (i.e. 1970–1980, 1972–
174 1982, ..., 2012–2022). Linear trend analysis was then used to calculate the decadal
175 trend. All significant significance tests were conducted using a two-sided Student's t-
176 test with a 0.05 (5%) critical level of significance.

177 2.4 Effect of spring variability on crop yield

178 To quantify the effect of spring variability on crop yield variability, a multi-param-
179 eter statistical model based on temperature and precipitation was constructed, using rice
180 as an example. This approach has been widely used in previous studies (Ray et al. 2015;
181 Ray et al. 2019; Vogel et al. 2019). Since the growth period of rice spans from March
182 to November, the effects of climate variability in spring, summer, and autumn are con-
183 sidered here. At the provincial level, the detrended rice yield anomalies were linearly
184 regressed against detrended climate anomalies, including mean temperature, tempera-
185 ture variability, mean precipitation and precipitation variability in spring, summer and
186 autumn. The full statistical model is expressed as:

$$\begin{aligned} 187 \text{ yield anomaly} = & \alpha_1 * Tmean_{MAM} + \alpha_2 * Tmean_{JJA} + \alpha_3 * Tmean_{SON} + \alpha_4 * Tstd_{MAM} + \alpha_5 \\ 188 & * Tstd_{JJA} + \alpha_6 * Tstd_{SON} + \alpha_7 * Pmean_{MAM} + \alpha_8 * Pmean_{JJA} + \alpha_9 \\ 189 & * Pmean_{SON} + \alpha_{10} * Pstd_{MAM} + \alpha_{11} * Pstd_{JJA} + \alpha_{12} * Pstd_{SON} \end{aligned}$$

190 Where T_{mean} and T_{std} denote the mean and standard deviation of temperature
191 for the special seasons, respectively. Here, yield anomalies are defined as the raw yields
192 minus a 9-year running mean, while climate variable anomalies are calculated by re-
193 moving the annual cycle from data with linear trends removed.

194 The overall R_2 of the equation represents the explained variance of climate varia-
195 bility on crop yield variability. A reduced statistical model was also constructed by
196 removing T_{std}_{MAM} and P_{std}_{MAM} from the full model. The contribution of climate vari-
197 ability to crop yield was quantified by calculating the difference in R_2 between the full
198 and reduced statistical models. In addition to the multi-parameter regression, ridge and
199 lasso regressions were also used to quantify the effects of spring variability, yielding
200 similar results. Therefore, only the multi-parameter regression results are shown in this
201 study.

202 **3. Climatological distribution of rapid temperature variability**

203 Figure 3 shows the climatology of STD and DTD in spring. The STD in southern
204 China exhibits a zonal distribution, with high values exceeding 3.5 °C in Guizhou–
205 Hunan–Jiangxi regions, and lower values located in the western parts of Yunnan and
206 Sichuan (Figure 3a). This distribution contrasts significantly with the pattern of cold
207 wave frequency in winter (Ma et al. 2022). There are notable differences in the monthly
208 evolution of STD. Compared to April and May, the STD in March is generally higher
209 and exhibits more pronounced spatial variability, with nearly 8% of stations exceeding
210 4.0 °C (Figure 3c), which is consistent with Figure 2. In terms of monthly spatial
211 distribution, the center of high values remains relatively stable over time and is
212 consistently located in the Guizhou–Hunan–Jiangxi region (Figure S1). This region is
213 the primary growing area for early rice cultivation, and as such, the risks associated
214 with spring temperature variability, such as late spring cold spells, should be closely
215 monitored and assessed in future agricultural planning and climate adaptation strategies.

216 As for DTD, its spatial distribution bears notable similarity to that of STD, with a
217 spatial correlation coefficient exceeding 0.88 (Figure 3b). However, in contrast to STD,
218 DTD remains relatively homogeneous from March to May, showing no significant
219 monthly variation, especially with small spatial differences between March and April
220 (Figure S1). Since STD is more sensitive to extreme values, the difference between
221 STD and DTD suggests that more extreme events occur in March than in April and May,
222 particularly rapid temperature change events.

223 Considering that STD and DTD alone cannot fully characterize extreme events in
224 spring, Figure 4 illustrates the frequency, mean intensity, and extreme intensity of RCE
225 using both relative and absolute threshold methods. The relative thresholds exhibit clear
226 spatial heterogeneity, with high value centers located in the Guizhou–Hunan–Jiangxi,
227 Anhui, and eastern Hubei. In these regions, only temperature drops exceeding -7°C can
228 be ranked within the top 10% in history, indicating that historical temperature drops are
229 notably larger here than those in surrounding areas. This distribution is consistent with
230 the patterns observed in STD and DTD. Meanwhile, the mean intensity and extreme
231 intensity in Figures 4b–c show similar spatial distributions with Figure 4a, confirming
232 that the spring temperature variability has the most severe impact on the Guizhou–
233 Hunan–Jiangxi region.

234 For the absolute threshold method, an average threshold of -6°C , derived from the
235 mean relative thresholds across all stations in Figure 4a (-5.98°C), was used to identify
236 RCE. Despite differences in case selection methods, the spatial distributions of
237 frequency, mean intensity, and extreme intensity of RCE (Figures 4d–f) remain
238 generally consistent with those of the relative threshold method. Since both methods
239 present consistent results in describing the characteristics of RCE, the absolute
240 threshold method will be used in the subsequent section.

241 Regarding the monthly evolution, the spatial distribution of RCE frequency exhibits
242 noticeable changes from March to May (Figure S2). The high-frequency center shifts

243 from the coastal region to the middle and lower reaches of the Yangtze River,
244 accompanied by a slight decrease in RCE days. By May, the frequency substantially
245 decreases across South China, except in the western Yunnan and Sichuan. This indicates
246 that spring disasters related to temperature variability in southern China are mainly
247 concentrated in early spring. As for the spatial distributions of mean and extreme
248 intensity, they do not differ obviously from March to May.

249 Figures 3 and 4 show that the temperature variability calculated by STD and DTD
250 aligns well with the distribution of RCE. To further establish their relationship, Figure
251 5 demonstrates the distribution of STD and RCE indices across 836 independent
252 stations. It is evident that the relative threshold decreases linearly as STD increases,
253 with the threshold dropping by 0.22 °C for each 0.1 °C rise in STD, suggesting a higher
254 likelihood of frequent and intense RCEs in the region. Notably, the frequency and
255 intensity of RCE also show a highly significant linear relationship with STD. Each
256 0.1°C rise in STD leads to an 11.2-day increase in frequency, as well as a 0.27°C and
257 0.29°C increase in mean and extreme intensity of RCE, respectively. Similar results are
258 observed between DTD versus RCE (Figure S3). These findings establish a stable linear
259 relationship between temperature variability and extreme events, especially for RCEs
260 in spring. This implies that the frequency and intensity of RCE in a region can be
261 estimated by straightforward calculations of STD or DTD in the future assessments.

262 Based on the above analysis on different aspects of rapid temperature variability, it
263 can be concluded that, although three methods were used for definition, STD, DTD and
264 RCE are robustly concentrated in the Guizhou–Hunan–Jiangxi region, with intensity
265 weakening over time in climatology. Furthermore, the frequency and intensity of RCE
266 can be effectively quantified by STD and DTD, providing a convenient method for
267 characterizing extreme temperature events.

268 **4. Decadal trends and causes for rapid temperature variability**

269 To examine changes in rapid temperature variability, the decadal trend in RCE-re-
270 lated characteristics is shown in Figure 6. From 1970 to 2022, the frequency of RCE
271 has increased in the Yangtze River Basin and Yunnan, with approximately 70% of the
272 stations in Sichuan, Chongqing, Hubei, Anhui, Jiangsu, and Yunnan passing the 95%
273 confidence level. The rates of increase in these provinces range from 0.1 to 1.8 days per
274 decade. Conversely, a decreasing trend is observed in South China, particularly in Gui-
275 zhou, Hunan, Jiangxi, Guangdong, Guangxi, Zhejiang, and Fujian, where rates range
276 from -0.5 to -1.0 days per decade (Figure 6a). The spatial distribution of RCE frequency
277 trend aligns well with its climatological pattern, that is, regions with higher climatolog-
278 ical frequencies tend to exhibit a decreasing trend, while regions with lower climato-
279 logical frequencies tend to show an increasing trend. It results in a distinct negative
280 correlation between decadal changes and the climatological distribution, with a corre-
281 lation coefficient reaching -0.34 for more than 800 independent samples (Figure 6d).
282 These findings demonstrate that the decadal trend of RCE frequency follows a pattern
283 of “stronger getting weaker, weaker getting stronger”.

284 Similar results are observed for the mean and extreme intensity of RCE. Specifically,
285 the mean intensity also demonstrates a decreasing trend in the Hunan–Jiangxi–Zhejiang
286 region, consistent with its climatological distribution. Although the correlation between
287 the climatological distribution and the mean intensity trend is modest at -0.11, it still
288 passes the 99% confidence test due to the independence of each station’s data. The de-
289 cadal trend of extreme intensity is more pronounced, with a decreasing trend observed
290 in Guizhou–Hunan–Jiangxi–Zhejiang. More than 64% of stations in these four prov-
291 inces pass the 95% confidence test. Therefore, the decadal trend of extreme intensity
292 corresponds better with the climatological distribution, with a correlation coefficient of
293 -0.31. It indicates that regions with high mean-state extreme intensity tend to experience
294 a weakening trend, and regions with weak mean-state extreme intensity tend to

295 experience a strengthening trend. Overall, these findings unveil a long-term trend pat-
296 tern in the frequency and intensity of RCE, characterized by a spatial distribution of
297 “stronger getting weaker, weaker getting stronger”.

298 To investigate the underlying mechanisms for the observed changes in RCE trends,
299 Figure 7 displays the corresponding trends in STD and DTD. Notably, the trend changes
300 in both STD and DTD share a similar spatial distribution with RCE, with a high spatial
301 correlation coefficient of 0.87. Specifically, both metrics demonstrate a downward trend
302 in South China, with over 70% of the stations in Guangxi, Guangdong, and Fujian pass-
303 ing the significance test. In the Yangtze River Basin and Yunnan Province, there is an
304 increasing trend, particularly in eastern Hubei, Anhui, and Jiangsu. This spatial distri-
305 bution closely aligns with the frequency of RCE, as evidenced by a robust linear rela-
306 tionship, indicated by a spatial correlation coefficient of 0.65. This suggests that the
307 observed trend changes in the frequency of RCE can largely be attributed to changes in
308 temperature variability. Specifically, an increase in temperature variability leads to a
309 rise in extreme events, subsequently elevating the frequency of RCEs. This is consistent
310 with the stable linear relationship depicted in Figure 5. Additionally, changes in DTD
311 trends can also help explain changes in RCE frequency (figure not shown).

312 To future unravel the possible drivers of the observed trends in temperature varia-
313 bility, Figure 8 presents the trend of mean temperature. It reveals that the warming rate
314 in South China is slower than in the Yangtze River Basin, with Guangxi, Guangdong,
315 and Fujian experiencing an average increase rate of 0.5–1.0°C per decade, considerably
316 lower than that of the Yangtze River Basin. Notably, the spatial pattern of mean tem-
317 perature trends closely matches those of STD and DTD. Regions with higher warming
318 rates correlate with increased STD, while areas with slower warming rates correspond
319 to decreased STD, yielding a correlation coefficient of 0.54. This finding suggests that
320 the observed changes in temperature variability trends are primarily driven by the spa-
321 tiotemporal heterogeneity in warming rates. This mechanism is in line with the

322 prevailing explanations (Chan et al. 2020; Tamarin-Brodsky et al. 2020), further em-
323 phasizing the role of local warming pattern in shaping regional temperature variability
324 changes.

325 In summary, the trend analysis indicates that the frequency and intensity of RCE
326 follow a spatial distribution characterized by “stronger getting weaker, weaker getting
327 stronger”. Specifically, there is a decreasing trend in South China and an increasing
328 trend in the Yangtze River Basin and Yunnan. The changes in the frequency and inten-
329 sity of RCE are mainly related to trend changes in STD and DTD, possibly driven by
330 the spatial non-uniformity of warming.

331 **5. Effects of variability on climate variations and crop yield**

332 Spring temperature variability significantly affects agriculture and society by alter-
333 ing key climate variables. To quantify these impacts, Figure 9 illustrates the associated
334 minimum temperature anomalies, precipitation, and wind speed during RCE. The anal-
335 ysis reveals that when RCEs occur, there is a 90% probability that the majority of sta-
336 tions will experience low temperatures, with minimum temperature anomalies dropping
337 below 0°C (Figure 9a). The mean intensity of minimum temperature anomalies across
338 provinces range from -1.0 to 6.4 °C, with notable high-value centers in the Guizhou–
339 Hunan–Jiangxi region. Extreme minimum temperature anomalies can reach as low as -
340 8 °C in Guizhou, Hunan, Jiangxi, Hubei, and Guangxi. This implies that RCEs are as-
341 sociated with severe cold weathers, potentially resulting in pronounced spring cold
342 spells.

343 In addition to extreme cold temperature anomalies, RCEs are often accompanied by
344 increased precipitation and gusty winds across most stations (Figures 9b–c). Specifi-
345 cally, the mean intensity of precipitation in southern China ranges from 5 to 18 mm/d,
346 with high-value centers concentrated at the intersection of Hubei, Jiangxi, and Anhui.
347 The extreme intensity of precipitation in these areas can reach up to 25 mm/d. Wind

348 speeds are similarly pronounced, with the highest recorded wind speed reaching 15 m/s
349 in Jiangsu.

350 In terms of sub-seasonal evolution, there is no significant difference in the occur-
351 rence frequency of minimum temperature anomalies, precipitation, and winds, all with
352 over 70% probability of occurrence during RCE (Figure 10). However, the intensity
353 shows pronounced sub-seasonal variations. Minimum temperature anomalies and gusty
354 winds are strongest in March and weaken as the month progresses. Precipitation, on the
355 contrary, peaks in May with an average of 20 mm, more than twice the average in March,
356 reflecting the sub-seasonal progression of the monsoon system in China (Ding and
357 Chan 2005; Yang et al. 2023). These findings suggest that RCEs are accompanied by
358 cold temperatures, precipitation and gusty winds, posing serious challenges for agricul-
359 tural and broader social production.

360 To quantify the impact of spring RCE on crop yields, a statistical model was con-
361 structed to assess the relationship between yield anomalies and climate factors, using
362 rice as an example. The climate factors include average anomalies of temperature and
363 precipitation, as well as seasonal variability throughout the entire reproductive period
364 of rice, totaling 12 elements. As depicted in Figure 11a, the explained variance of the
365 statistical model across 13 provinces reveals that climate factors account for 19–49%
366 of yield variability. Notably, Hubei and Guangdong contribute approximately 40%,
367 while Sichuan shows a comparatively lower contribution. These findings align with
368 previous results indicating that climate variability explains nearly one-third of the var-
369 iability in crop yields (Ray et al. 2019; Vogel et al. 2019).

370 A reduced statistical model was constructed to quantify the contribution of spring
371 temperature and precipitation variability by removing them from the 12 elements. The
372 difference in the explained variance between the full and reduced statistical models is
373 displayed in Figure 11b. The values across the 13 provinces range from 1%–11%, with
374 a mean value of 4%. Higher values are observed in Yunan, Guizhou, Hunan, Hubei, and
375 Anhui. This suggests that spring temperature variability and its associated climatic

376 impacts can account for roughly 4% of the variance in rice yield anomalies in southern
377 China. In addition, the sensitivity to spring variability varies considerably from prov-
378 ince to province, which may be related to local cropping systems, water and fertilizer
379 management practices, and sowing varieties.

380 **6. Conclusion and Discussion**

381 This study explores the characteristics, trends and mechanisms of rapid temperature
382 variability and quantifies its impact on crop yields. From various perspectives, rapid
383 temperature variability is measured in terms of standard deviation of daily temperature
384 (STD), day-to-day temperature variability (DTD) and rapid cooling event (RCE). These
385 indices show a consistent climatological pattern for spring temperature variability, with
386 greater variability and more frequent and stronger RCEs observed in the Guizhou–
387 Hunan–Jiangxi region. Despite differences in calculation methods, the frequency and
388 intensity of RCEs exhibit strong linear relationships with both STD and DTD.
389 Specifically, an increase of 0.1°C in STD correlates with an 11.2-day increase in RCE
390 frequency, alongside increases of 0.27°C and 0.29°C in mean and extreme intensity,
391 respectively. Thus, temperature variability serves as a reliable indicator of RCE
392 characteristics.

393 Over the past half century, the spatial distribution of long-term trends in rapid
394 temperature variability across southern China reveals significant heterogeneity.
395 Specifically, RCEs have become more frequent and intense in the Yangtze River Basin
396 and Yunnan. Over these provinces, the frequency of RCEs in spring has increased by
397 0.1 to 1.8 days per decade, while the extreme intensity of RCEs has grown by 0.9 to
398 2.7 °C per decade. Conversely, the frequency and intensity of RCEs exhibit a negative
399 trend across most of South China. This trend pattern aligns with the overall
400 climatological distribution, following a ‘stronger getting weaker, weaker getting
401 stronger’ pattern. The observed trends in RCEs are mainly related to the trend changes
402 in STD and DTD, which is driven by spatial non-uniformity in warming. This finding
403 highlights an important consideration that although global warming has enabled the
404 possibility of earlier rice sowing (Olesen et al. 2012; Fatima et al. 2020; Minoli et al.
405 2022), the increased variability in spring temperatures introduces a heightened risk for

406 crop failure. Therefore, the spring temperature variability deserves more attention in
407 agricultural production.

408 Rapid temperature variability has profound implications for both agriculture and
409 society by altering key climate variables. RCEs are frequently accompanied by low
410 temperatures, precipitation, and gusty winds, which can severely impact agricultural
411 productivity and social stability. Our statistical model demonstrates that climate factors,
412 including mean climate as well as climate variability—explain 19%–49% of the
413 variance in rice yield anomalies. Although the quantified contributions are not directly
414 comparable across studies due to differences in regional contexts and methodologies,
415 the influence of climate factors on yield variability is consistent with previous findings,
416 which suggested that climate factors explain approximately one-third of crop yield
417 variations (Ray et al. 2015).

418 Moreover, we demonstrate that spring variability associated with climate extremes
419 contributes up to 11% of the explained variance in rice yield anomalies. This
420 contribution is lower than the 26% attributed to climate variability in a previous study
421 (Vogel et al. 2019), likely because this study focuses specifically on spring rather than
422 full-season variability. Our results also indicate that summer variability contributes
423 more significantly than spring and autumn variability (results not shown), which may
424 be due to the greater sensitivity of rice to extreme heat waves and heat stress during the
425 flowering and filling periods (Wang et al. 2019; Song et al. 2022). Additionally, this
426 study centers on local regions rather than national or global scales, recognizing that the
427 influence of climate variability on yield variability can differ substantially across
428 regions due to disparities in agricultural practices, climatic conditions, and crop
429 management (Heino et al. 2018; Anderson et al. 2019; Lesk et al. 2022). To build on
430 this work, future research could broaden the geographic scope to encompass diverse
431 regions and agricultural systems, which would provide a more comprehensive
432 understanding of climate impacts on crops. Additionally, exploring the dynamic
433 mechanisms of changes in temperature variability and crop responses through general
434 circulation model simulations will be crucial. Such approaches can enhance predictive
435 ability, helping to inform region-specific adaptation strategies and increase agricultural
436 resilience to climate extremes.

437

438

439 **Acknowledgements**

440 This work was supported by the Natural Science Foundation of Hubei Province,
441 China (Program No. 2024AFB115) and the Fundamental Research Funds for the
442 Central Universities (Program No. 2662024ZKQD003).

443 **Data Availability**

444 The meteorological station data is available at <https://data.cma.cn>. The yield and
445 area data are freely available at <https://data.stats.gov.cn/easyquery.htm?cn=E0103>. The
446 analysis scripts are available upon request from the corresponding author.

447

448 **Reference:**

- 449 Alexander, L. V., 2016: Global observed long-term changes in temperature and
450 precipitation extremes: A review of progress and limitations in ipcc assessments
451 and beyond. *Weather Clim. Extreme.*, **11**, 4-16,
452 <https://doi.org/10.1016/j.wace.2015.10.007>.
- 453 Allstadt, A. J., S. J. Vavrus, P. J. Heglund, A. M. Pidgeon, W. E. Thogmartin, and V. C.
454 Radeloff, 2015: Spring plant phenology and false springs in the conterminous
455 us during the 21st century. *Environ. Res. Lett.*, **10**, 104008,
456 <https://doi.org/10.1088/1748-9326/10/10/104008>.
- 457 ANDERSON, W. B., R. SEAGER, W. BAETHGEN, M. CANE, and L. YOU, 2019:
458 Synchronous crop failures and climate-forced production variability. *Sci. Adv.*,
459 **5**, <https://doi.org/10.1126/sciadv.aaw1976>.
- 460 Baffour-Ata, F., P. Antwi-Agyei, E. Nkiaka, A. J. Dougill, A. K. Anning, and S. O.
461 Kwakye, 2021: Effect of climate variability on yields of selected staple food
462 crops in northern ghana. *J. Agr. Food Res.*, **6**, 100205,
463 <https://doi.org/10.1016/j.jafr.2021.100205>.
- 464 Bathiany, S., V. Dakos, M. Scheffer, and T. M. Lenton, 2018: Climate models predict
465 increasing temperature variability in poor countries. *Sci. Adv.*, **4**, eaar5809,
466 <https://doi.org/10.1126/sciadv.aar5809>.
- 467 Blackport, R., J. C. Fyfe, and J. A. Screen, 2021: Decreasing subseasonal temperature
468 variability in the northern extratropics attributed to human influence. *Nat.*
469 *Geosci.*, **14**, 719-723, <https://doi.org/10.1038/s41561-021-00826-w>.
- 470 Cao, L., Y. Zhu, G. Tang, F. Yuan, and Z. Yan, 2016: Climatic warming in China
471 according to a homogenized data set from 2419 stations: Climatic warming in
472 china. *Int. J. Climatol.*, **36**, 4384-4392, <https://doi.org/10.1002/joc.4639>.
- 473 Chamberlain, C. J., B. I. Cook, I. García De Cortázar-Atauri, and E. M. Wolkovich,
474 2019: Rethinking false spring risk. *Global Change Biol.*, **25**, 2209-2220,
475 <https://doi.org/10.1111/gcb.14642>.

476 Chan, D., A. Cobb, L. R. V. Zeppetello, D. S. Battisti, and P. Huybers, 2020:
477 Summertime temperature variability increases with local warming in
478 midlatitude regions. *Geophys. Res. Lett.*, **47**, e2020GL087624,
479 <https://doi.org/10.1029/2020GL087624>.

480 Cui, Z., and C. He, 2023: Decadal trend of synoptic temperature variability over the
481 northern hemisphere in winter. *Theor. Appl. Climatol.*, **152**, 829-842,
482 <https://doi.org/10.1007/s00704-023-04423-2>.

483 Dai, A., and J. Deng, 2021: Arctic amplification weakens the variability of daily
484 temperatures over northern middle-high latitudes. *J. Climate*, **34**, 2591-2609,
485 <https://doi.org/10.1175/JCLI-D-20-0514.1>.

486 Ding, Y., and J. C. L. Chan, 2005: The East Asian summer monsoon: An overview.
487 *Meteor. Atmos. Phys.*, **89**, 117–142, <https://doi.org/10.1007/s00703-005-0125-z>.

488 Fatima, Z., and et al. , 2020: The fingerprints of climate warming on cereal crops
489 phenology and adaptation options. *Sci. Rep.*, **10**,
490 <https://doi.org/10.1038/s41598-020-74740-3>.

491 Fischer, E. M., J. Rajczak, and C. Schär, 2012: Changes in european summer
492 temperature variability revisited. *Geophys. Res. Lett.*, **39**, L19702,
493 <https://doi.org/10.1029/2012GL052730>.

494 Garner, A. J., and D. P. Duran, 2024: Late-winter and springtime temperature variations
495 throughout new jersey in a warming climate. *J. Appl. Meteorol. Clim.*, **63**, 197-
496 207, <https://doi.org/10.1175/JAMC-D-23-0152.1>.

497 Ge, J., Q. Liu, B. Zan, Z. Lin, S. Lu, B. Qiu, and W. Guo, 2022: Deforestation intensifies
498 daily temperature variability in the northern extratropics. *Nat. Commun.*, **13**,
499 5955, <https://doi.org/10.1038/s41467-022-33622-0>.

500 Gough, W. A., 2008: Theoretical considerations of day-to-day temperature variability
501 applied to toronto and calgary, canada data. *Theor. Appl. Climatol.*, **94**, 97-105,
502 <https://doi.org/10.1007/s00704-007-0346-9>.

503 Han, J., S. Fang, X. Wang, W. Zhuo, Y. Yu, X. Peng, and Y. Zhang, 2024: The impact
504 of intra-annual temperature fluctuations on agricultural temperature extreme
505 events and attribution analysis in mainland China. *Sci. Total Environ.*, **949**,
506 174904, <https://doi.org/10.1016/j.scitotenv.2024.174904>.

507 He, Y., X. Wang, B. Zhang, Z. Wang, and S. Wang, 2023: Contrast responses of strong
508 and weak winter extreme cold events in the northern hemisphere to global
509 warming. *Climate Dyn.*, **61**, 4533-4550, [https://doi.org/10.1007/s00382-023-](https://doi.org/10.1007/s00382-023-06822-7)
510 [06822-7](https://doi.org/10.1007/s00382-023-06822-7).

511 Healy, J. P., and et al. , 2023: Seasonal temperature variability and mortality in the
512 medicare population. *Environ. Health Persp.*, **131**, 077002,
513 <https://doi.org/10.1289/EHP11588>.

514 Heinicke, S., K. Frieler, J. Jägermeyr, and M. Mengel, 2022: Global gridded crop
515 models underestimate yield responses to droughts and heatwaves. *Environ. Res.*
516 *Lett.*, **17**, 044026, <https://doi.org/10.1088/1748-9326/ac592e>.

517 Heino, M., M. J. Puma, P. J. Ward, D. Gerten, V. Heck, S. Siebert, and M. Kummu,
518 2018: Two-thirds of global cropland area impacted by climate oscillations. *Nat*
519 *Commun*, **9**, 1257, <https://doi.org/10.1038/s41467-017-02071-5>.

520 Holmes, C. R., T. Woollings, E. Hawkins, and H. De Vries, 2016: Robust future changes
521 in temperature variability under greenhouse gas forcing and the relationship
522 with thermal advection. *J. Climate*, **29**, 2221-2236,
523 <https://doi.org/10.1175/JCLI-D-14-00735.1>.

524 Kotz, M., L. Wenz, A. Stechemesser, M. Kalkuhl, and A. Levermann, 2021: Day-to-
525 day temperature variability reduces economic growth. *Nat. Climate Change*, **11**,
526 319-325, <https://doi.org/10.1038/s41558-020-00985-5>.

527 Krauskopf, T., and R. Huth, 2024: Trends in intraseasonal temperature variability in
528 europe: Comparison of station data with gridded data and reanalyses. *Int. J.*
529 *Climatol.*, **44**, 3054-3074, <https://doi.org/10.1002/joc.8512>.

530 Lesk, C., and W. Anderson, 2021: Decadal variability modulates trends in concurrent
531 heat and drought over global croplands. *Environ. Res. Lett.*, **16**, 055024,
532 <https://doi.org/10.1088/1748-9326/abeb35>.

533 Lesk, C., and et al. , 2022: Compound heat and moisture extreme impacts on global
534 crop yields under climate change. *Nat. Rev. Earth Env.*, **3**, 872-889,
535 <https://doi.org/10.1038/s43017-022-00368-8>.

536 Li, J., and D. W. J. Thompson, 2021: Widespread changes in surface temperature
537 persistence under climate change. *Nature*, **599**, 425-430,
538 <https://doi.org/10.1038/s41586-021-03943-z>.

539 Lin, F., and et al. , 2023: Late spring cold reduces grain number at various spike
540 positions by regulating spike growth and assimilate distribution in winter wheat.
541 *Crop J.*, **11**, 1272-1278, <https://doi.org/10.1016/j.cj.2023.03.014>.

542 Ma, L., Z. Wei, and X. Li, 2022: Spatial and temporal characteristics of various cold
543 surges over China during 1962–2018. *Int. J. Climatol.*, **42**, 10253-10267,
544 <https://doi.org/10.1002/joc.7896>.

545 Minoli, S., J. Jägermeyr, S. Asseng, A. Urfels, and C. Müller, 2022: Global crop yields
546 can be lifted by timely adaptation of growing periods to climate change. *Nat.*
547 *Commun.*, **13**, <https://doi.org/10.1038/s41467-022-34411-5>.

548 Olesen, J. E., and et al. , 2012: Changes in time of sowing, flowering and maturity of
549 cereals in europe under climate change. *Food Additives and Contaminants Part*
550 *a-Chemistry Analysis Control Exposure & Risk Assessment*, **29**, 1527-1542,
551 <https://doi.org/10.1080/19440049.2012.712060>.

552 Olonscheck, D., A. P. Schurer, L. Lücke, and G. C. Hegerl, 2021: Large-scale
553 emergence of regional changes in year-to-year temperature variability by the
554 end of the 21st century. *Nat. Commun.*, **12**, 7237,
555 <https://doi.org/10.1038/s41467-021-27515-x>.

556 Pane, M. M., and R. E. Davis, 2024: The association between short-term temperature
557 variability and mortality in virginia. *PLOS ONE*, **19**, e0310545,
558 <https://doi.org/10.1371/journal.pone.0310545>.

559 Park, T.-W., C.-H. Ho, S.-J. Jeong, Y.-S. Choi, S. K. Park, and C.-K. Song, 2011:
560 Different characteristics of cold day and cold surge frequency over East Asia in
561 a global warming situation. *J. Geophys. Res.*, **116**, D12118,
562 <https://doi.org/10.1029/2010JD015369>.

563 Perkins-Kirkpatrick, S. E., and P. B. Gibson, 2017: Changes in regional heatwave
564 characteristics as a function of increasing global temperature. *Sci. Rep.*, **7**,
565 12256, <https://doi.org/10.1038/s41598-017-12520-2>.

566 Ray, D. K., J. S. Gerber, G. K. MacDonald, and P. C. West, 2015: Climate variation
567 explains a third of global crop yield variability. *Nat. Commun.*, **6**, 5989,
568 <https://doi.org/10.1038/ncomms6989>.

569 Ray, D. K., P. C. West, M. Clark, J. S. Gerber, A. V. Prishchepov, and S. Chatterjee,
570 2019: Climate change has likely already affected global food production. *Plos*
571 *One*, **14**, e0217148, <https://doi.org/10.1371/journal.pone.0217148>.

572 Rezaei, E. E., and et al. , 2023: Climate change impacts on crop yields. *Nat. Rev. Earth*
573 *Env.*, **4**, 831-846, <https://doi.org/10.1038/s43017-023-00491-0>.

574 Rhines, A., K. A. McKinnon, M. P. Tingley, and P. Huybers, 2017: Seasonally resolved
575 distributional trends of North american temperatures show contraction of winter
576 variability. *J. Climate*, **30**, 1139-1157, [https://doi.org/10.1175/JCLI-D-16-](https://doi.org/10.1175/JCLI-D-16-0363.1)
577 [0363.1](https://doi.org/10.1175/JCLI-D-16-0363.1).

578 Samset, B. H., C. Zhou, J. S. Fuglestedt, M. T. Lund, J. Marotzke, and M. D. Zelinka,
579 2023: Steady global surface warming from 1973 to 2022 but increased warming
580 rate after 1990. *Commun. Earth Environ.*, **4**, 400,
581 <https://doi.org/10.1038/s43247-023-01061-4>.

582 Schär, C., P. L. Vidale, D. Lüthi, C. Frei, C. Häberli, M. A. Liniger, and C. Appenzeller,
583 2004: The role of increasing temperature variability in european summer
584 heatwaves. *Nature*, **427**, 332-336, <https://doi.org/10.1038/nature02300>.

585 Schneider, T., T. Bischoff, and H. Płotka, 2015: Physics of changes in synoptic
586 midlatitude temperature variability. *J. Climate*, **28**, 2312-2331,
587 <https://doi.org/10.1175/JCLI-D-14-00632.1>.

588 Screen, J. A., 2014: Arctic amplification decreases temperature variance in northern
589 mid- to high-latitudes. *Nat. Climate Change*, **4**, 577-582,
590 <https://doi.org/10.1038/nclimate2268>.

591 Song, Y. L., and et al. , 2022: The negative impact of increasing temperatures on rice
592 yields in southern China. *Sci. Total Environ.*, **820**,
593 <https://doi.org/10.1016/j.scitotenv.2022.153262>.

594 Tamarin-Brodsky, T., K. Hodges, B. J. Hoskins, and T. G. Shepherd, 2020: Changes in
595 northern hemisphere temperature variability shaped by regional warming
596 patterns. *Nat. Geosci.*, **13**, 414-421, [https://doi.org/10.1038/s41561-020-0576-](https://doi.org/10.1038/s41561-020-0576-3)
597 [3](https://doi.org/10.1038/s41561-020-0576-3).

598 Van Der Wiel, K., and R. Bintanja, 2021: Contribution of climatic changes in mean and
599 variability to monthly temperature and precipitation extremes. *Commun. Earth*
600 *Environ.*, **2**, 1, <https://doi.org/10.1038/s43247-020-00077-4>.

601 Vogel, E., and et al. , 2019: The effects of climate extremes on global agricultural yields.
602 *Environ. Res. Lett.*, **14**, 054010, <https://doi.org/10.1088/1748-9326/ab154b>.

603 Wang, Y. L., and et al. , 2019: Research progress on heat stress of rice at flowering stage.
604 *Rice Science*, **26**, 1-10, <https://doi.org/10.1016/j.rsci.2018.06.009>.

605 Wei, J., W. Q. Han, W. G. Wang, L. Zhang, and B. Rajagopalan, 2023: Intensification
606 of heatwaves in China in recent decades: Roles of climate modes. *Npj Clim.*
607 *Atmos. Sci.*, **6**, 98, <https://doi.org/10.1038/s41612-023-00428-w>.

608 Xiao, L., and et al. , 2018: Estimating spring frost and its impact on yield across winter
609 wheat in China. *Agr. Forest Meteorol.*, **260-261**, 154-164,
610 <https://doi.org/10.1016/j.agrformet.2018.06.006>.

611 Xu, Z., F. Huang, Q. Liu, and C. Fu, 2020: Global pattern of historical and future
612 changes in rapid temperature variability. *Environ. Res. Lett.*, **15**, 124073,
613 <https://doi.org/10.1088/1748-9326/abccf3>.

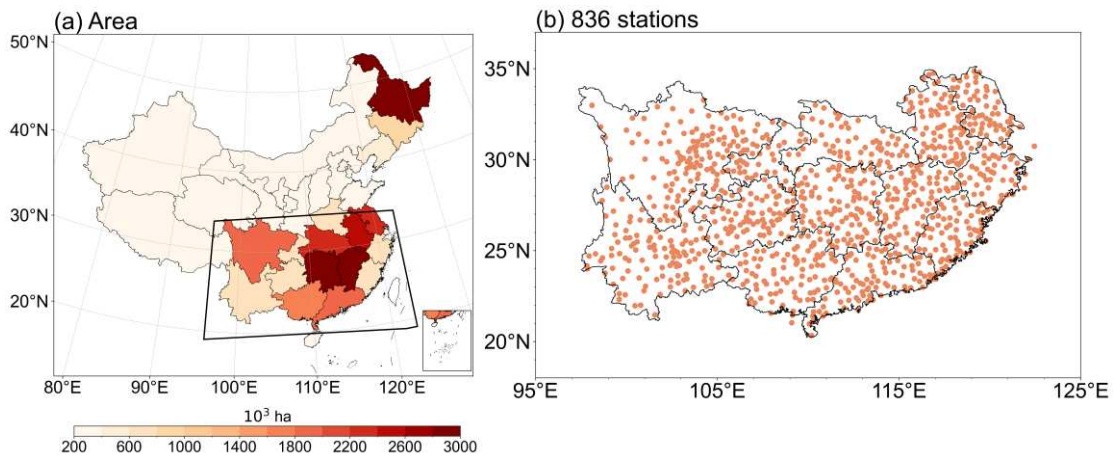
614 Yang, X., P. Huang, P. Hu, and Z. Wang, 2023: Distinct impacts of two types of summer
615 ENSO with different temporal evolutions on the Asian summer monsoon: Role
616 of the tropical Indo-western Pacific. *J. Climate*, **36**, 3917–3936,
617 <https://doi.org/10.1175/JCLI-D-22-0532.1>.

618 Zhu, Y.-L., H.-J. Wang, T. Wang, and D. Guo, 2018: Extreme spring cold spells in North
619 China during 1961–2014 and the evolving processes. *Atmos. Ocean. Sci. Lett.*,
620 **11**, 432-437, <https://doi.org/10.1080/16742834.2018.1514937>.

621

622

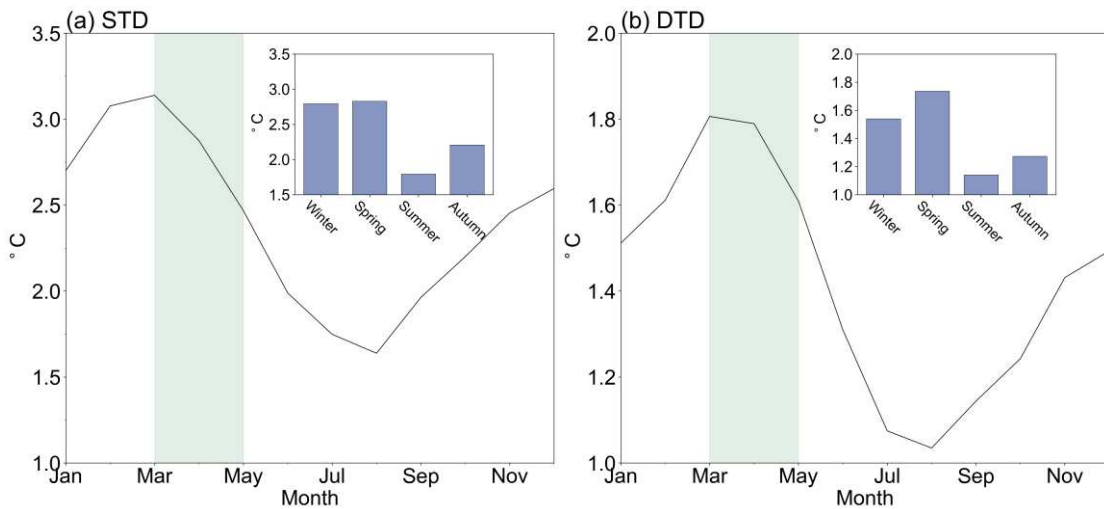
623



624

625 **Figure1 The study area in southern China.** (a) Spatial distribution of average rice
626 planting area in recent five years. The black box in (a) represents the southern China
627 domain. (b) Distribution of 725 meteorological stations in southern China.

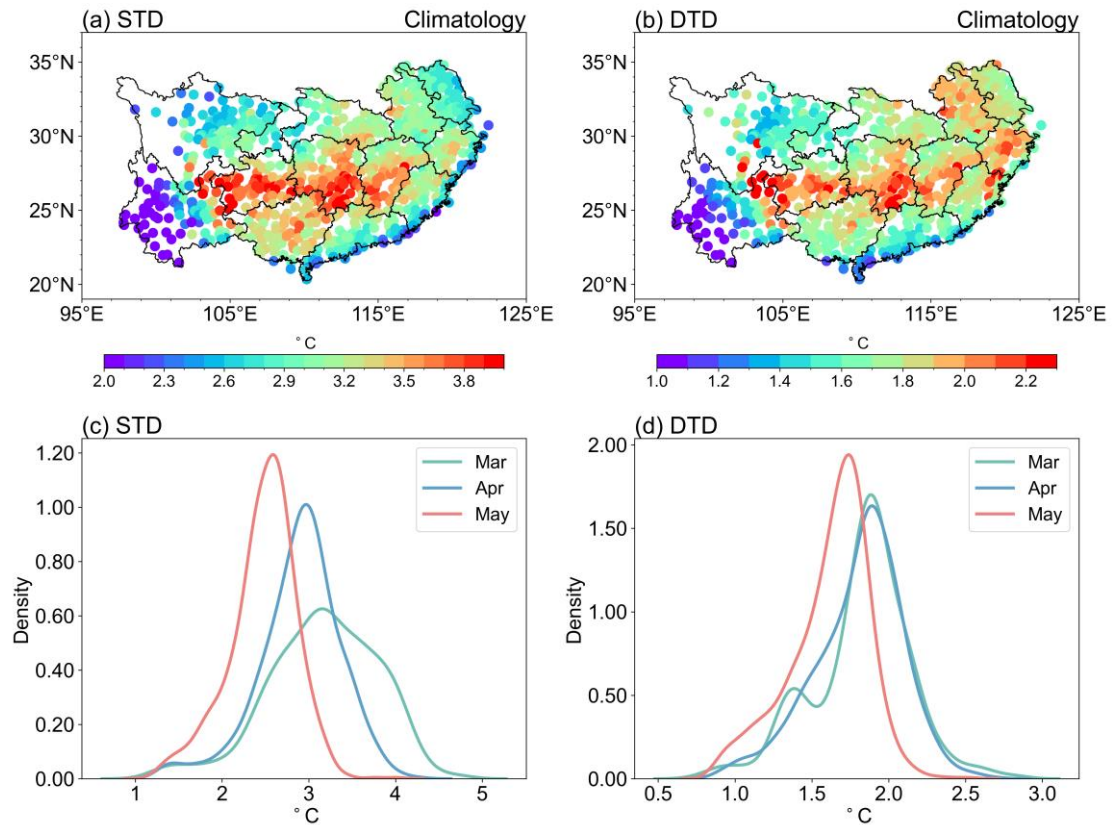
628



629

630 **Figure 1 Monthly and seasonal evolution of temperature variability.** (a) The black
631 line indicates the multi-year monthly standard deviation of daily temperature from 1970
632 to 2022. The bar chart represents the multi-year seasonal standard deviation. The light-
633 grey shade indicates March to May. (b) as in (a), but for DTD.

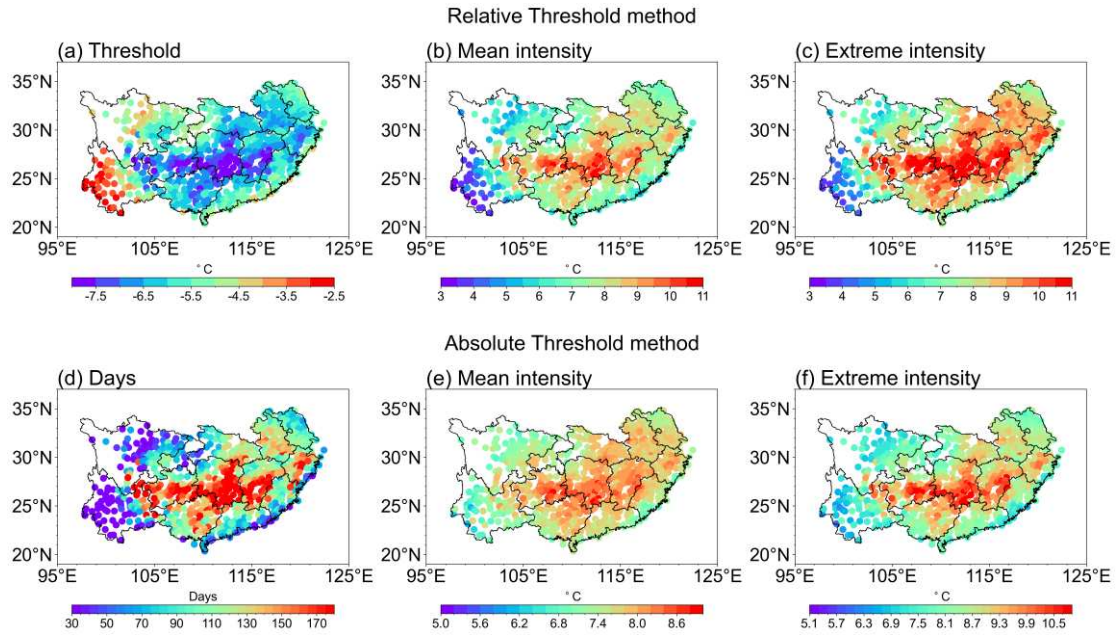
634



635

636 **Figure 3 Climatology of STD and DTD.** Spring mean (a) STD and (b) DTD of daily
 637 temperature in southern China from 1970 to 2022. Probability density functions of
 638 monthly (c) STD and (d) DTD fitted by kernel density estimation for 836 meteorolog-
 639 ical stations in southern China.

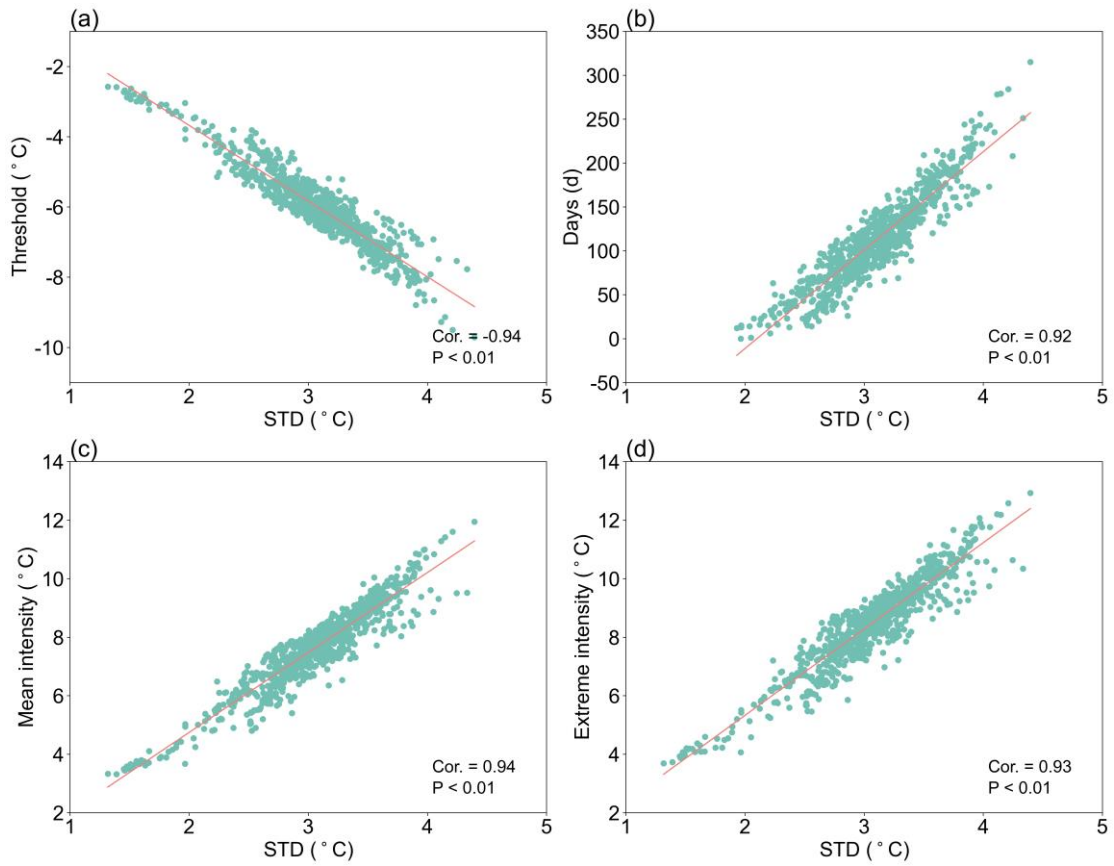
640



641

642 **Figure 4 Characteristics of rapid cooling events.** Spatial distribution of (a) relative
 643 threshold, and seasonal means of (b) mean intensity as well as (c) extreme intensity of
 644 RCE from 1970 to 2022 based on the relative threshold method. (d-f) as in (a-c), but
 645 for days, mean intensity and extreme intensity based on the absolute threshold method.

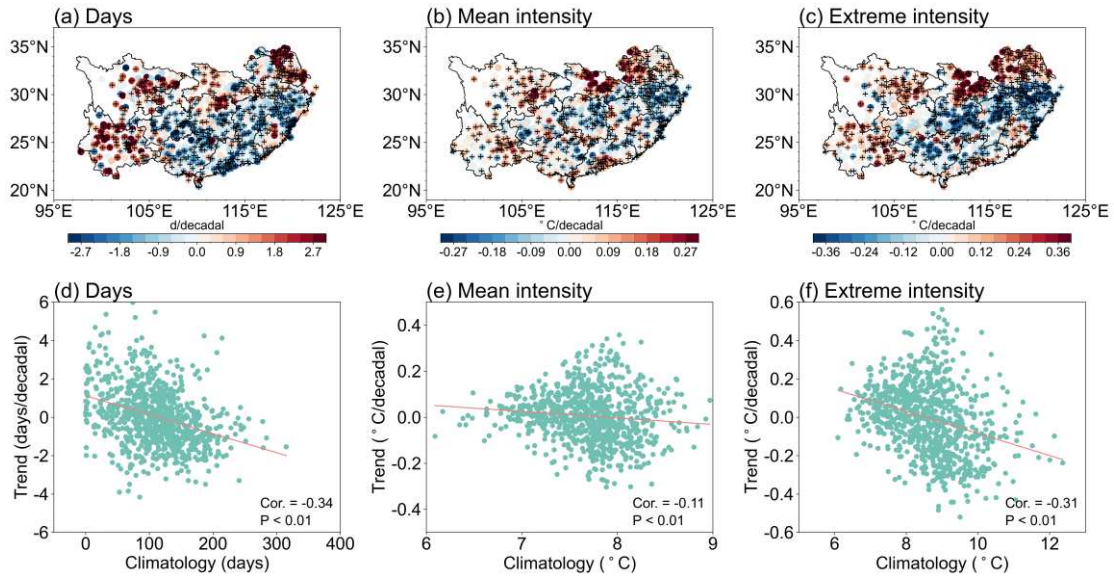
646



647

648 **Figure 5 Relationship between STD and RCE.** Scatter plots for regional averaged
 649 spring STD and (a) threshold, (b) days, (c) mean intensity and (d) extreme intensity of
 650 RCE from 1970 to 2022 across 836 meteorological stations in southern China. The
 651 leastsquares fitting line is shown as the black line in each panel. Correlation coefficients
 652 and p-value are labelled in the lower left of each panel.

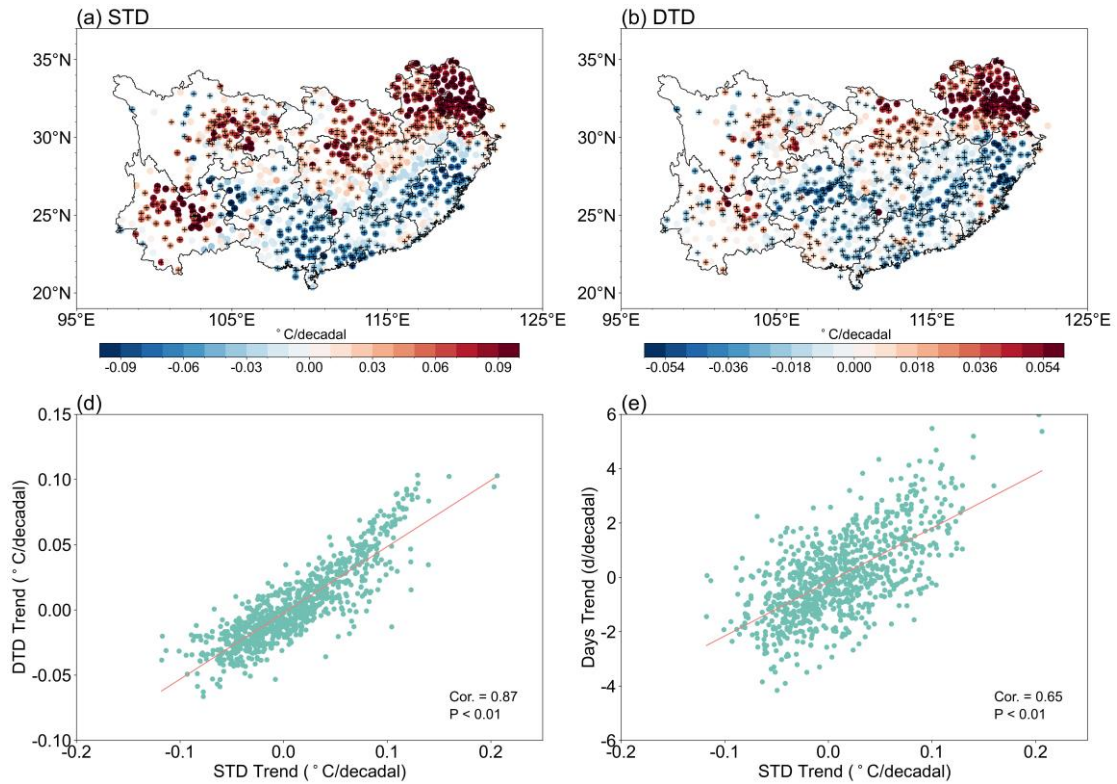
653



654

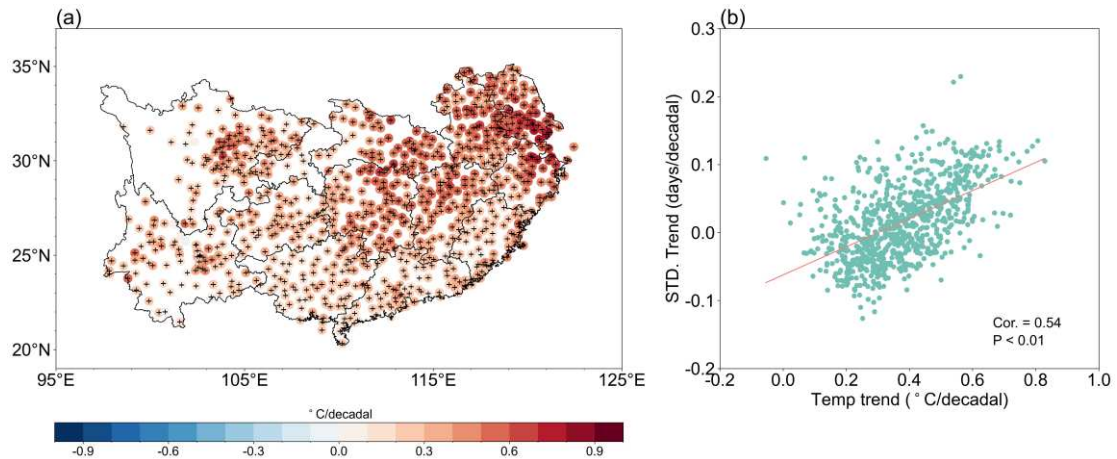
655 **Figure 6 Decadal trend of characteristics related to RCE.** The decadal trend of (a)
 656 days, (b) mean intensity, (c) extreme intensity of RCE from 1970 to 2022. A plus sign
 657 denotes statistical significance exceeding the 95% confidence level. The relationship
 658 between trend in (d) days, (e) mean intensity, (f) extreme intensity and their climatology
 659 for 836 meteorological stations. The least squares fitting line is shown as the black line
 660 in each panel. Correlation coefficients and p-value are labelled in the lower right of
 661 each panel.

662



663

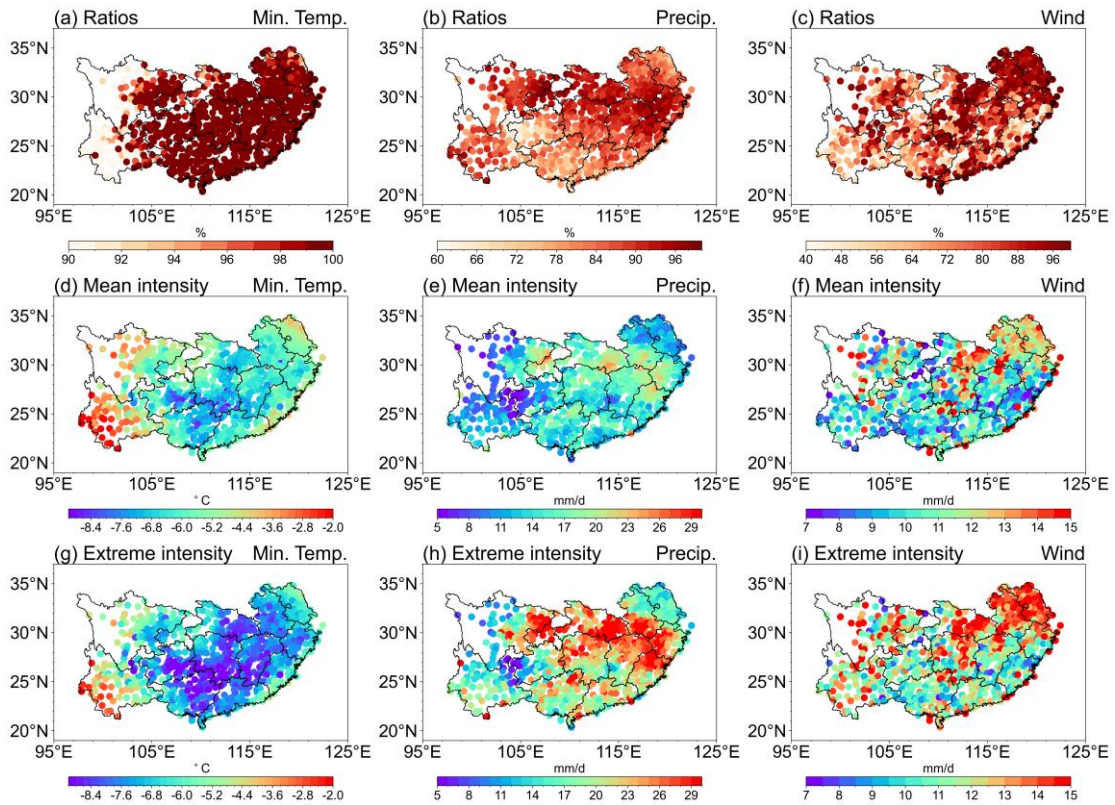
664 **Figure 7 Decadal trend of STD and DTD.** (a, b) as in Figure 6 (a, b, c), but for the
 665 results of STD and DTD. (c, d) as in Figure 6 (d, e, f), but for the relationship between
 666 (c) STD trend and DTD trend, and (d) STD trend and day trend for 836 meteorological
 667 stations.



668

669 **Figure 8 Decadal trend of mean temperature.** (a) as in Figure 6 (a), but for the results
 670 of spring mean temperature. (b) as in Figure 6 (d), but for the relationship between STD
 671 trend and mean temperature trend.

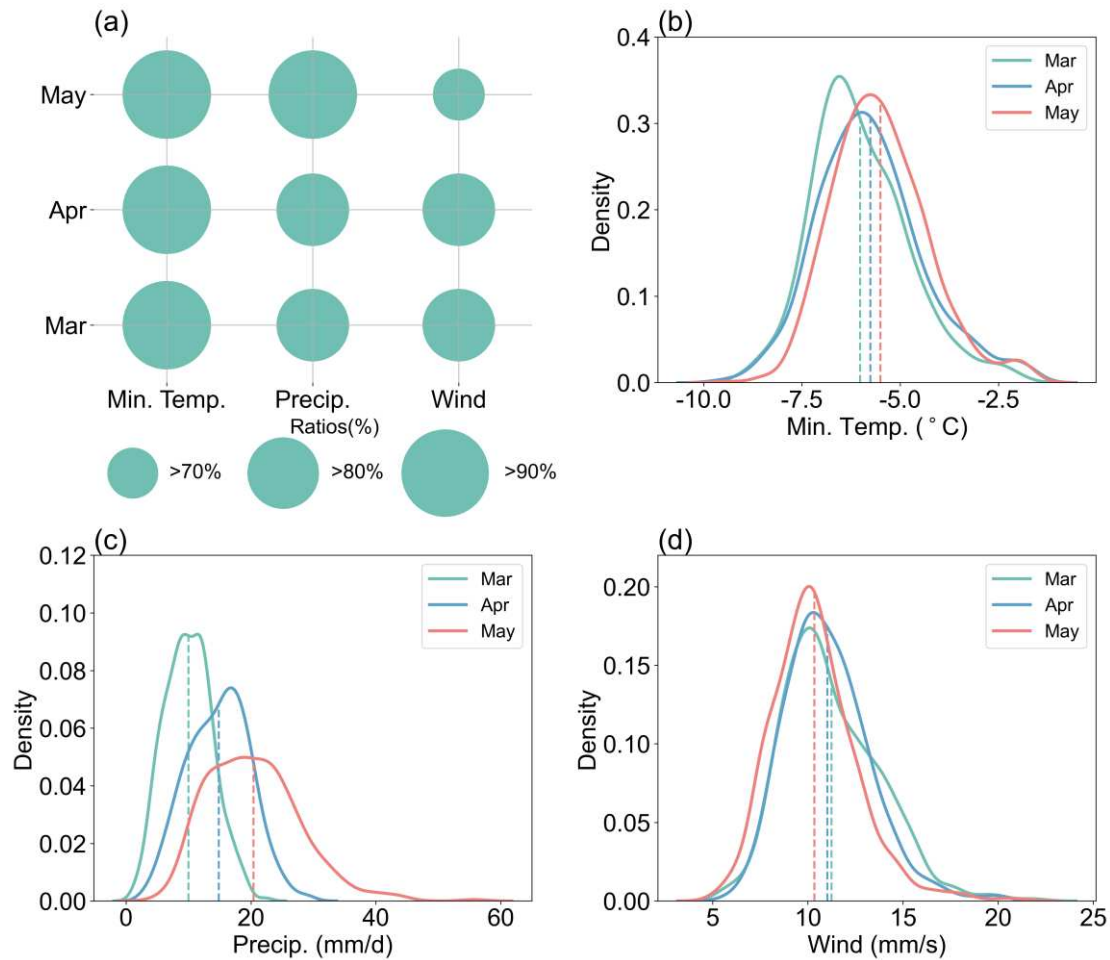
672



673

674 **Figure 9 Characteristics of climate variables related to RCE.** Spatial distribution
 675 of (a) frequency ratio, (d) mean intensity and (g) extreme intensity of minimum tem-
 676 peratures anomalies below 0°C during RCE from 1970 to 2022. Anomalies are calcu-
 677 lated with annual cycle removed. (b, e, h) as in (a, d, g), but for results with precipitation
 678 exceeding 1 mm/d. (c, f, i) as in (a, d, g), but for results with wind speed exceeding 7
 679 m/s.

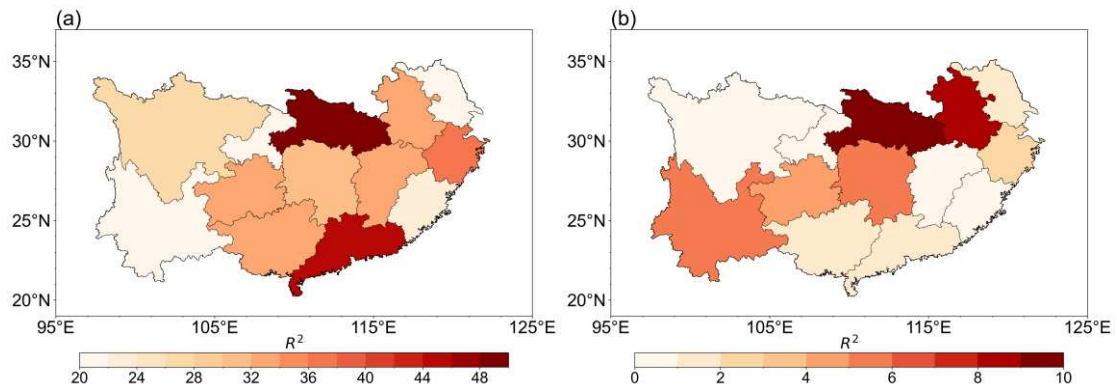
680



681

682 **Figure 10 Monthly characteristics related to RCE.** (a) The average frequency pro-
 683 portion of RCEs where the minimum temperature anomalies, precipitation and
 684 wind speed exceeded the corresponding thresholds during March–May in southern China,
 685 respectively. The threshold of the minimum temperature anomalies is less than 0°C, and
 686 the threshold of precipitation and wind speed is greater than 1mm/d and greater than 7
 687 m/s. Probability density functions of monthly (b) minimum temperature anomalies, (c)
 688 precipitation and (d) wind speed related to RCE for 836 meteorological stations during
 689 March–May in southern China. The light green, light blue and light red dotted lines
 690 represent the average of 836 stations in March, April and May, respectively.

691



692

693 **Figure 11 Explained variation for rice yield anomalies.** (a) R^2 values of the full
 694 statistical model accounting for mean climate conditions and climate variability. (b)
 695 Difference in R^2 of full statistical model and reduced model, estimating the partial ex-
 696 plained variance from spring climate variability. R^2 values are calculated from the ex-
 697 plained variance of the multiple regression of rice yield anomalies against climate var-
 698 iable anomalies.

699

700

Supplementary Materials

Decadal trend of spring rapid temperature variability and its impact on yield over southern China

Xianke Yang¹, Yixuan Zhang, Haosu Tang³, Ping Huang², Xiaoxia Ling¹, Shaobing Peng¹, Dongliang Xiong^{1,*}

1. MARA Key Laboratory of Crop Ecophysiology and Farming System in the Middle
9 Reaches of the Yangtze River, Huazhong Agricultural University, Wuhan, Hubei,
430070, 10 China

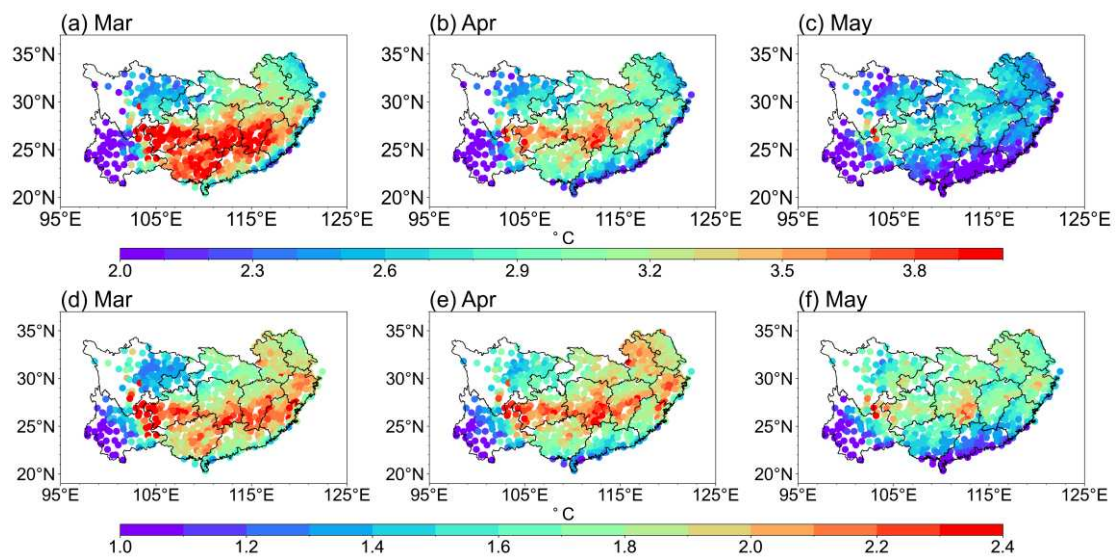
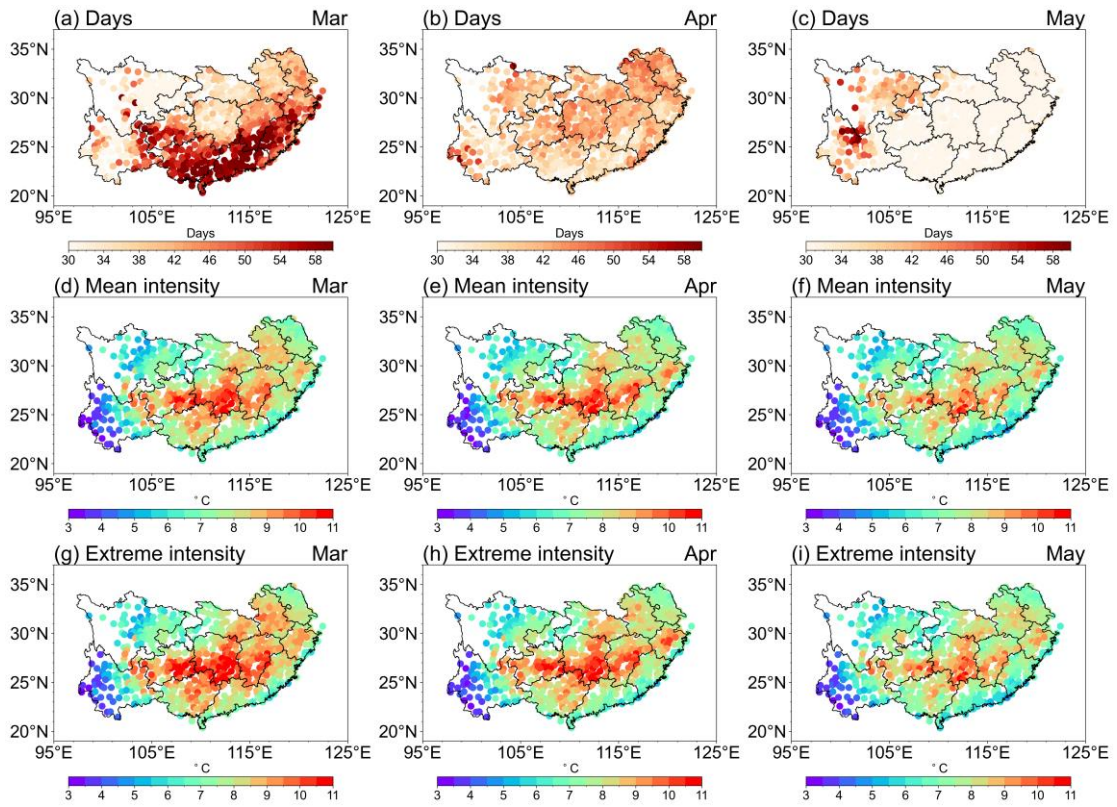


Figure S1. Spatial distributions of monthly means of (a–c) STD and (d–f) DTD during March–May from 1970 to 2022.

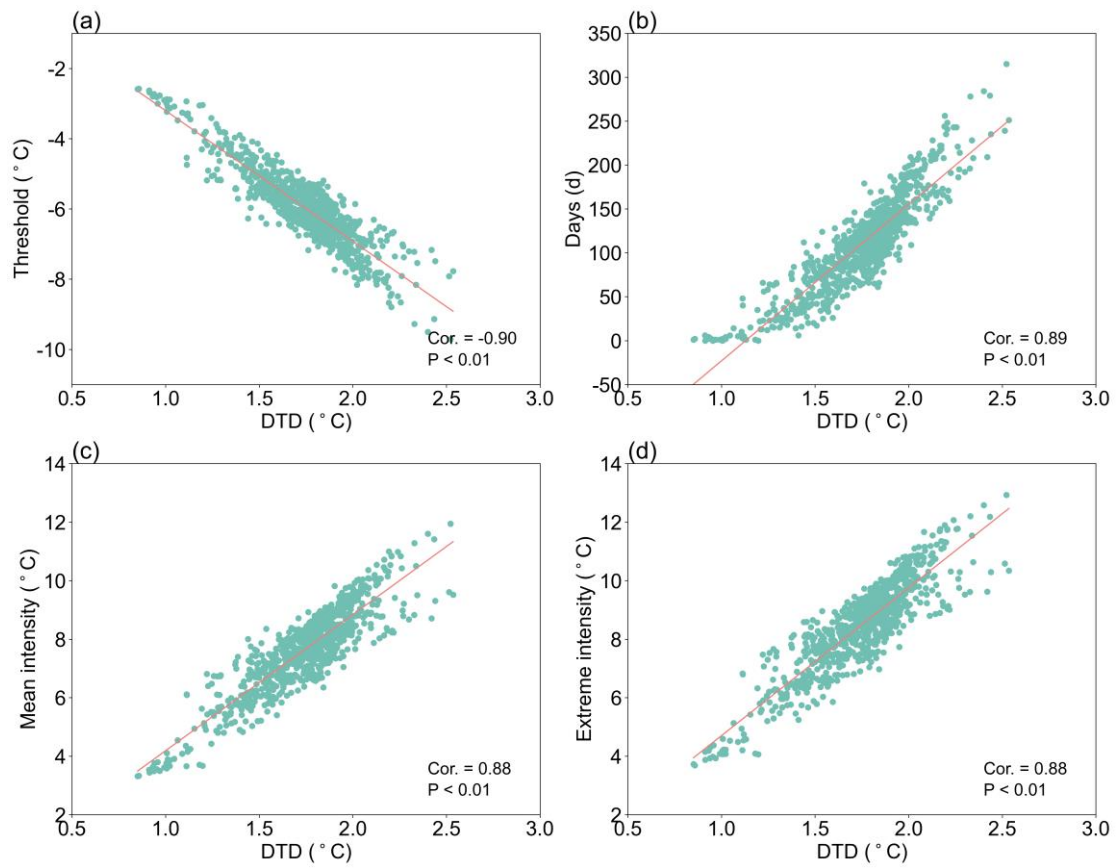


714

715 **Figure S2.** Spatial distributions of monthly means of (a–c) days, (d–f) mean intensity
 716 and (g–i) extreme intensity of RCE during March–May from 1970 to 2022.

717

718



719

720 **Figure S3.** As in Figure 5, but for relationship between DTD and RCE.

721

722